Single-Atom Verification of the Optimal Trade-Off between Speed and Cost in Shortcuts to Adiabaticity

J.-W. Zhang[1,*], J.-T. Bu,[2,3,*] J. C. Li[4,1,*] Weiquan Meng[5,*] W.-Q. Ding,[2,3] B. Wang[2,3] W.-F. Yuan,[2,3] H.-J. Du,[2,3] G.-Y. Ding,[2,3] W.-J. Chen,[2,3] L. Chen[2,1] F. Zhou,[2,1,†] Zhenyu Xu[5,‡] and M. Feng[1,2,6,§]

[1]*Research Center for Quantum Precision Measurement, Guangzhou Institute of Industry Technology, Guangzhou 511458, China*
[2]*State Key Laboratory of Magnetic Resonance and Atomic and Molecular Physics, Wuhan Institute of Physics and Mathematics, Innovation Academy of Precision Measurement Science and Technology, Chinese Academy of Sciences, Wuhan 430071, China*
[3]*School of Physics, University of the Chinese Academy of Sciences, Beijing 100049, China*
[4]*Guangzhou Institute of Industrial Intelligence, Guangzhou 511458, China*
[5]*School of Physical Science and Technology, Soochow University, Suzhou 215006, China*
[6]*Department of Physics, Zhejiang Normal University, Jinhua 321004, China*

The approach of shortcuts to adiabaticity enables the effective execution of adiabatic dynamics in quantum information processing with enhanced speed. Owing to the inherent trade-off between dynamical speed and the cost associated with the transitionless driving field, executing arbitrarily fast operations becomes impractical. To understand the accurate interplay between speed and energetic cost in this process, we propose theoretically and verify experimentally a new trade-off, which is characterized by a tightly optimized bound within s-parametrized phase spaces. Our experiment is carried out in a single ultracold $^{40}Ca^+$ ion trapped in a harmonic potential. By exactly operating the quantum states of the ion, we execute the Landau-Zener model as an example, where the quantum speed limit as well as the cost are governed by the spectral gap. We witness that our proposed trade-off is indeed tight in scenarios involving both initially eigenstates and initially thermal equilibrium states. Our work helps understanding the fundamental constraints in shortcuts to adiabaticity and illuminates the potential of underutilized phase spaces that have been traditionally overlooked.

Adiabatic dynamics requires an exceptionally slow evolution of quantum states, posing challenges for practical applications of quantum technology, which are strongly restricted by decoherence time. Fortunately, shortcuts to adiabaticity offers a pathway to achieving identical outcomes through expedited processes [1]. Transitionless quantum driving exemplifies such techniques [2–4], whose core principle is to involve an ancillary counterdiabatic field $H_1(t)$ within $t \in (0, \tau)$. Under the combined Hamiltonian $H(t) = H_0(t) + H_1(t)$, the fast quantum dynamics aligns with the adiabatic process governed solely by $H_0(t)$. This quantum technology has been extensively employed to enhance the performance of elementary operations in quantum information science [5–17], and applied to other research fields, such as quantum thermodynamics [18–25], quantum metrology [26], and even the population engineering of organisms in medical biology [27].

One natural question: what is the maximum speed achievable by such transitionless driving? Given the inherent trade-offs, a quantum speed limit (QSL) necessarily constrains the rapidity of this transitionless driving. A seminal relationship between the cost rate and evolution speed has been established [18], indicating that instantaneous manipulation remains elusive owing to the requirement of an infinite cost rate. However, establishing a direct relationship between the dynamical speed and the driving cost often encounters obstacles, leading to the prevalent use of the upper bound of dynamical speed, namely, the QSL, to associate with the cost rate. Thus, the tightness of this bound and its ability to accurately reflect the true dynamical process emerge as two critical factors in assessing the precision of the trade-off between speed and cost.

Experimentally exploring such relationship is imperative and typical advancements of QSL experiments so far include detection of speedup in optical cavity QED systems [28], observation crossover between Mandelstam-Tamm and Margolus-Levitin bounds using fast matter wave interferometry [29], navigation of quantum brachistochrones between distant states of an atom across optical lattices [30], and execution of logical gates at the QSL in superconducting transmons [31].

In this Letter, we propose and also verify experimentally a new trade-off between speed and cost, based on an optimized QSL bound using the s-parametrized phase space technique [32]. This approach yields a tight bound compared to those derived in Wigner phase space or Hilbert space. We demonstrate that this new trade-off surpasses the one outlined in [18] that actually lacks tightness [33]. We also justify our findings experimentally in an ion trap platform using the well-known Landau-Zener (LZ) model,

which is closely related to the Ising model [34–36] and thus useful for quantum annealing [37]. In this context, our present study substantially enhances the understanding of fundamental constraints governing the speed of quantum operations. Notably, the tight QSL bound we investigate here outperforms the traditionally employed Wigner, Glauber-Sudarshan, and Husimi phase spaces. This finding strongly supports the notion that rarely used phase spaces may offer superior performance in certain quantum tasks.

To clarify this new trade-off, we first elucidate briefly the theory of the cost rate, quantum dynamical speed and limit. Consider a time-dependent Hamiltonian $H_0(t)$, characterized by its instantaneous eigenvalues $\{\epsilon_n(t)\}$ and eigenstates $\{|n_t\rangle\}$. In ideal situation, the adiabatic dynamics takes an infinitely long time and would not induce transitions between the eigenstates. In contrast, for a swift evolution in transitionless quantum driving without eigenstate transitions, it is necessary to apply an ancillary counterdiabatic field with the form of $H_1(t) = i\hbar[\partial_t(|n_t\rangle\langle n_t|), |n_t\rangle\langle n_t|]$ [1].

A suite of cost rate functions for transitionless driving has been presented [38]. Notably, the most elementary among them, when disregarding the setup constant, takes the following subsequent form [18] as

$$\partial_t C = \|H_1(t)\| = \sqrt{2}\hbar\sqrt{\langle\partial_t n_t|\partial_t n_t\rangle}, \quad (1)$$

where $\|X\| = \sqrt{\mathrm{tr}(X^\dagger X)}$ denotes the Frobenius norm of the operator X [39].

In the study of dynamical speed, it is commonly characterized by the time derivative of a metric that denotes the overlap or disparity between an initial and its subsequent evolved state [40]. In this Letter, we utilize the relative purity [41], a metric known for its computational efficiency, denoted by $P_t(\rho_0, \rho_t) = \mathrm{tr}(\rho_0\rho_t)/\mathrm{tr}(\rho_0^2)$ [42] or simply $P_t(\rho_0, \rho_t) = \mathrm{tr}(\rho_0\rho_t)$ [43,44]. Throughout this work, we will adopt the latter to assess the QSL. However, the upper bound of evolution speed determined via such relative purity is not tight [33]. Fortunately, this limitation can be effectively circumvented through the application of the recently developed s-parametrized phase space technique in the context of QSL [32].

The relative purity in s-parametrized phase space is expressed as $P_t(\rho_0, \rho_t) = \int d\mu(\eta)F_{\rho_0}^{-s}(\eta)F_{\rho_t}^s(\eta)$ [32], where $F_A^s(\eta)$ is the phase space function of operator A, η is a point in a phase space that determines the state $|\eta\rangle\langle\eta| (\eta \to |\eta\rangle)$ in Hilbert space, and the index s labels a family of Cahill-Glauber phase spaces [45,46]. To acquire an optimal bound, the changing rate of the relative purity, namely, the dynamical speed, is bounded by

$$|\dot{P}_t(\rho_0, \rho_t)| \leq \sup_{s \in S} V_{\mathrm{QSL}}^s(t), \quad (2)$$

where $V_{\mathrm{QSL}}^s(t) = [\int d\mu(\eta)F_{\rho_0}^{-s}(\eta)^2 \int d\mu(\eta')|\dot{F}_{\rho_t}^s(\eta')|^2]^{1/2}$ [32] represents the QSL in Cahill-Glauber s-parametrized phase

space, and sup signifies the least upper bound, related to the phase space parameter s within a set S. Notably, $s = 0, 1$, and -1 correspond to the well-known Wigner, Glauber-Sudarshan, and Husimi phase spaces, respectively [47,48].

Without loss of generality, let us consider N-level quantum systems. The least upper bound, i.e., Eq. (2), is achieved when $s \to -\infty$ and the tightness of such bound is ensured by the condition of

$$b_\mu(0) \propto h_\nu(t)b_\lambda(t)f_{\nu\lambda\mu}, \quad (3)$$

where $b_\mu(t) = 2\mathrm{tr}(\rho_t T_\mu)$, $h_\mu(t) = 2\mathrm{tr}(H(t)T_\mu)$, $f_{\nu\lambda\mu}$ are totally antisymmetric regarding the interchange of any pair of its indices, and T_μ are the generators of SU(N) Lie algebra. The summation over repeated Greek indices is implicit.

Proof.—To prove the condition stated in Eq. (3) for ensuring the tightness of the QSL upper bound in Eq. (2), it is essential to demonstrate that $F_{\rho_0}^{-s}(\eta)$ and $\dot{F}_{\rho_t}^s(\eta)$ are linearly dependent. For N-level quantum systems, we have $F_{\rho_0}^{-s}(\eta) = 1/N + 2b_\mu(0)r_{-s}R_\mu$ and $\dot{F}_{\rho_t}^s(\eta) = (2/\hbar)r_s b_\mu(t)h_\nu(t)R_\lambda f_{\nu\mu\lambda}$ [33], where $r_s = \sqrt{(N+1)^{1+s}}/2$ ($s \in \mathbb{R}$), and $R_\mu = \langle\eta|T_\mu|\eta\rangle$. As s approaches $-\infty$, the value of r_{-s} tends towards infinity. Consequently, the first term, $1/N$, in $F_{\rho_0}^{-s}(\eta)$ becomes negligible and can be omitted. Thus, we can solve the set of simultaneous equations, i.e., Eq. (3) to ensure linear relevance between $F_{\rho_0}^{-s}(\eta)$ and $\dot{F}_{\rho_t}^s(\eta)$, and thereby guaranteeing the tightness of the upper bound in Eq. (2). More details can be found in [33]. ∎

In this Letter, we focus on two-level (qubit) systems for experimental verification. $V_{\mathrm{QSL}}^s(t)$ in Eq. (2) is simplified as [32]

$$V_{\mathrm{QSL}}^s(t) = \frac{1}{2\hbar}\sqrt{3^s + |\vec{b}_0|^2}|\vec{h}_t \times \vec{b}_t|, \quad (4)$$

where $\vec{b}_t = \mathrm{tr}(\rho_t\vec{\sigma})$ and $\vec{h}_t = \mathrm{tr}(H(t)\vec{\sigma})$. When the initial state is pure, we have $\Delta E = \frac{1}{2}|\vec{h}_t \times \vec{b}_t|$ and $|\vec{b}_0|^2 = 1$. Thus, the s-parametrized QSL bound of the qubit system in Eq. (4) is rewritten as $V_{\mathrm{QSL}}^s(t) = \sqrt{1 + 3^s}\Delta E/\hbar$, which is a Mandelstam-Tamm type bound [49]. In certain specialized scenarios, such as a qubit system initially prepared in one of the eigenstates of $H_0(0)$, we may discern analytically the relationship between the speed limit and the cost rate. After some algebra, Eq. (4) becomes $V_{\mathrm{QSL}}^s(t) = \sqrt{3^s + 1}\sqrt{\langle\partial_t n_t|\partial_t n_t\rangle}$, which leads to a new concise trade-off between the QSL and the cost rate

$$\frac{V_{\mathrm{QSL}}^s(t)}{\partial_t C} = \frac{\sqrt{3^s + 1}}{\sqrt{2}\hbar}, \quad (5)$$

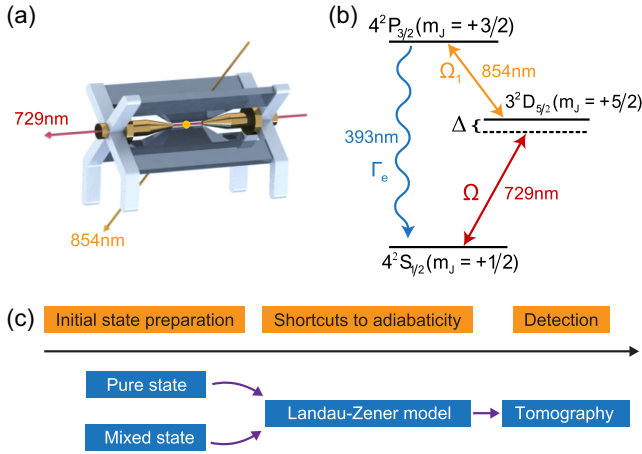governed by the s parameters in phase spaces. Clearly, the optimal trade-off between the true dynamical speed and

FIG. 1. (a) The ion trap system, where the 729-nm laser beam is in parallel with the axial direction, and the 854-nm laser irradiates with an angle 45° with respect to the axial direction. (b) Level scheme of the $^{40}Ca^+$ ion, where the double-sided arrows and the wavy arrow represent the laser irradiation and dissipation, respectively. (c) The experimental steps starting from the initialization to the final detection.

cost rate is upper bounded by $|\dot{P}_t|/\partial_t C \le V_{QSL}^{-\infty}(t)/\partial_t C = 1/\sqrt{2}\hbar$ [50].

In the remainder of this Letter, we will verify experimentally the proposed trade-off in the ion-trap platform, using the LZ model under various initial states. Our experiment is carried out with a single ultracold $^{40}Ca^+$ ion confined in a linear Paul trap, see Fig. 1(a), whose axial and radial frequencies are, respectively, $\omega_z/2\pi = 1.01$ and $\omega_r/2\pi = 1.2$ MHz under the pseudopotential approximation. The quantization axis is defined by a magnetic field of approximately 6 G at the trap center, which is with respect to the axial direction at an angle 45°. Prior to the experiment, we have cooled the ion down to near the ground state of the vibrational modes by Doppler and resolved sideband cooling, which is sufficient to avoid detrimental effects of vibrational modes on our operations.

As plotted in Fig. 1(b), we encode the qubit in electronic states $|4^2S_{1/2}, m_J = +1/2\rangle$ (labeled as $|g\rangle$) and $|3^2D_{5/2}, m_J = +5/2\rangle$ (labeled as $|e\rangle$) with m_J the magnetic quantum number, and the qubit is manipulated by an ultrastable narrow linewidth 729-nm laser with the Lamb-Dicke parameter ~ 0.1. As elucidated below, we will consider experimentally both the initially prepared eigenstate and the initially prepared thermal equilibrium state (TES), i.e., $\rho^{eg}(0) = \exp[-\beta H_0(0)]/Z_0$ with the partition function $Z_0 = tr\{\exp[-\beta H_0(0)]\}$ and $\beta = 1/k_BT$ (where T denotes the temperature and k_B is Boltzmann constant). For the latter case, we need to introduce an extra energy level $|4^2P_{3/2}, m_J = +3/2\rangle$ (labeled as $|p\rangle$) for initial state preparation. $|p\rangle$ couples to $|e\rangle$ by a 854-nm laser (with Rabi frequency Ω_1) and dissipates to $|g\rangle$ with the decay rate of $\Gamma_e/2\pi = 23.1$ MHz. Using this dissipative channel,

we can rapidly acquire the required TES via reinforcement learning [33].

Figure 1(c) plots the scheme of our experimental steps for implementing a LZ model. Here the LZ model is described by $H_0(t) = \Delta\sigma_x + g(t)\sigma_z$, where Δ is the energy splitting, $g(t)$ is the time-dependent field, and $\sigma_{i\in(x,z)}$ is the Pauli operator. The instantaneous eigenstates of LZ are $|\psi_-(t)\rangle = \sin[\theta(t)]|g\rangle - \cos[\theta(t)]|e\rangle$ and $|\psi_+(t)\rangle = \cos[\theta(t)]|g\rangle + \sin[\theta(t)]|e\rangle$ with $\cos[2\theta(t)] = g(t)/\sqrt{g^2(t) + \Delta}$ and $\sin[2\theta(t)] = \Delta/\sqrt{g^2(t) + \Delta}$. According to Ref. [4], the corresponding ancillary counterdiabatic term is given by

$$H_1(t) = -\frac{\hbar g'(t)\Delta}{2[\Delta^2 + g^2(t)]}\sigma_y, \qquad (6)$$

which allows us to investigate Eqs. (4) and (5). Thus, the combined Hamiltonian is $H(t) = H_0(t) + H_1(t)$ and can be rewritten as

$$H(t) = \tilde{\Omega}(t)(e^{i\tilde{\varphi}(t)}\sigma_+ + e^{-i\tilde{\varphi}(t)}\sigma_-) + g(t)\sigma_z. \qquad (7)$$

Equation (7) is a modified form of the LZ model with the effective Rabi frequency $\tilde{\Omega}(t) = \sqrt{4\Delta^2 + (\Xi)^2}$ and the phase $\tilde{\varphi}(t) = \arctan[\Xi/(2\Delta)]$, where $\Xi = -(\hbar g'(t)\Delta/2[\Delta^2 + g^2(t)])$. So our LZ model can be carried out by exactly controlling the irradiation power and the phase of 729-nm laser, under the government of Eq. (7).

Here we first verify the proposed trade-off from the initially prepared pure state, i.e., an eigenstate $|\psi_+(0)\rangle$. In this case, with the counterdiabatic field, i.e., Eq. (6) applied, the system evolves around the instantaneous eigenstate $|\psi_+(t)\rangle$. For the condition far from the adiabatic limit, we choose $\Delta = \Omega_0/4$ and $g(t) = (\Omega_0/2)\cos(\pi t/\tau)$ with $\Omega_0/2\pi = 40$ kHz, and consider various time periods τ. For an intuitive comparison of QSL and cost rate, we set $\hbar = 1$. Figures 2(a) and 2(b) plot the theoretical simulation of the QSL based on Eqs. (1) and (4), including V_{QSL}^s with Wigner phase space $s = 0$ or $s = -\infty$ and the cost rate $\partial_t C$. It is evident that $V_{QSL}^{s=0}$ is less accurate for shorter time period, indicating that $V_{QSL}^{s=-\infty}$ is better for describing the QSL in the case of short time periods. Comparing Figs. 2(a) and 2(b), we see that the cost rate varies consistently with the speed, showing that faster manipulation requires higher energy consumption.

Experimentally, we focus on the case of $\tau = 50$ μs. The initial state $|\psi_+(0)\rangle$ is prepared by applying a carrier-transition pulse with $\theta = 0.8524\pi$ and $\tilde{\varphi} = \pi/2$. Variation of the characteristic parameters of the LZ model is made by operational sequences with 20 steps, as sketched in Fig. 2(c). The powers, frequencies, and phases of the lasers are controlled via acousto-optic modulators and an arbitrary waveform generator. After applying the laser pulses, we measure the population in the excited state $|e\rangle$ in three
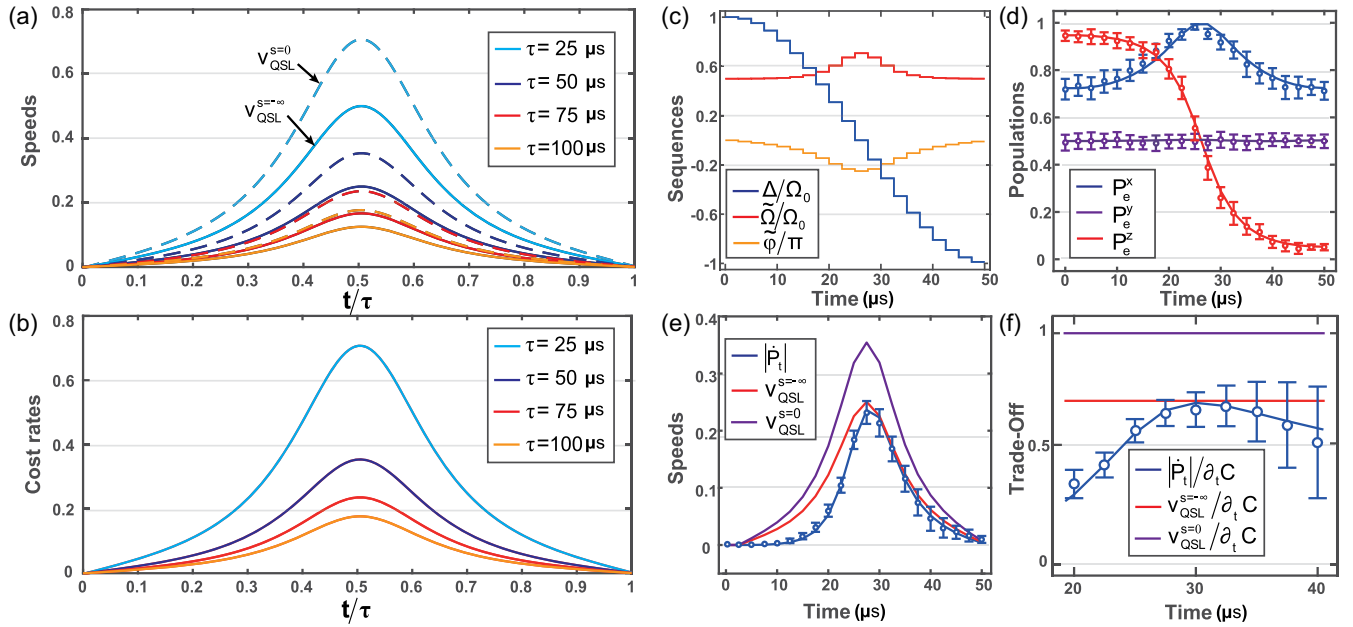
FIG. 2. Trade-off between speed and cost in shortcuts to adiabaticity for an initially prepared eigenstate. Panels (a),(b) display theoretical analyses over varying time periods from $\tau = 25$ to 100 μs, while panels (c)–(f) depict experimental implementations with a fixed time period of 50 μs. (a) Time evolution of speed with respect to various time periods τ, where dashed and solid lines, respectively, represent $V_{\mathrm{QSL}}^{s=0}$ and $V_{\mathrm{QSL}}^{s=-\infty}$. Cases of time periods are colored differently. (b) Time evolution of cost rate $\partial_t C$ versus various time periods τ, where cases of time periods are colored differently. (c) Applied 20-step sequences (with each of 2.5 μs) for the laser detuning Δ, the effective Rabi frequency strength $\tilde{\Omega}$ and the effective phase $\tilde{\varphi}$. (d) Time evolution of the populations P_e^x, P_e^y, and P_e^z as defined in [33]. (e) Time evolution of the actual dynamic speed $|\dot{P}_t|$ in comparison to the two cases of QSL, i.e., $V_{\mathrm{QSL}}^{s=0}$ and $V_{\mathrm{QSL}}^{s=-\infty}$. (f) Time evolution of the actual trade-off $|\dot{P}_t|/\partial_t C$ in comparison to $V_{\mathrm{QSL}}^{s=0}/\partial_t C$ and $V_{\mathrm{QSL}}^{s=-\infty}/\partial_t C$ within the LZ crossing time window. Dots indicate experimental results, while solid lines represent theoretical predictions. Error bars, reflecting the statistical standard deviation, are derived from 50 000 measurements for each data point.

directions, labeled as $P_e^{i \in (x,y,z)}$, which constructs the quantum tomographic results of ρ_t [33], see Fig. 2(d).

To examine the optimal QSL, we compare the results from Eq. (4) to the actual dynamical speed of the quantum state, i.e., $|\dot{P}_t| = |\mathrm{tr}(\rho_0 \dot{\rho}_t)| = \frac{1}{\hbar}|\mathrm{tr}(\rho_0 H(t)\rho_t) - \mathrm{tr}(\rho_0 \rho_t H(t))|$ with $\rho_0 = |\psi_+(0)\rangle\langle\psi_+(0)|$. Figure 2(e) presents the experimentally measured dynamical speed $|\dot{P}_t|$, facilitating a comparison with the QSL employing various phase space parameters, such as $s = -\infty$ and $s = 0$ (Wigner phase space). We find that, although both $V_{\mathrm{QSL}}^{s=-\infty}$ and $V_{\mathrm{QSL}}^{s=0}$ have maximal values at $t = 27.5$ μs, varying consistently with $|\dot{P}_t|$, the former is tight at $t = 29$ μs (see proof in Ref. [33]), indicating that $V_{\mathrm{QSL}}^{s=-\infty}$ represents the optimal QSL we acquired. This optimality hinges on two factors: one being the tightness of the bound, and the other its ability to accurately reflect the actual dynamical speed.

Based on the optimal QSL, we are ready to examine the optimal trade-off, i.e., Eq. (5), as illustrated in Fig. 2(f). Note that, although the upper bound of $V_{\mathrm{QSL}}^{s=-\infty}$ matches very well the experimentally actual dynamical speed, the deviation between the two curves is evident in the regime of $t < 29$ μs, see Fig. 2(e). We emphasize that the difference originates from the fact that the QSL curves are nearly

symmetric whereas the curve of the experimental actual dynamical speed is not [51]. Besides, for the experimental data, the error bars of the data points after $t = 30$ μs become larger and larger with time, which reflect more imprecision and uncertainty involved in the measurement. We conjecture that the enlarged uncertainty comes from the emergence of the complex dynamics when the state evolves through the avoided crossing area (around 29 μs) of the LZ model. This uncertainty is amplified in Fig. 2(f) by the cost rate $\partial_t C$ whose values are rapidly shrinking with $t > 29$ μs. Consequently, to verify the optimal trade-off more accurately, it is highly expected to detect the spin states with ultimate precision.

Next, we consider a more complex situation, verifying the trade-off in the case of an initially prepared mixed state, i.e., a TES. For simplicity of our experimental implementation, we fix the inverse temperature $\beta\Omega_0 = 5 \times 10^{28}$. Similar to the above case for initially prepared pure state, we design the operational sequences with 20 steps to vary the characteristic parameters of the LZ model, as sketched in Fig. 3(a), and with the laser pulses we measure the quantum tomographic results of ρ_t, see Fig. 3(b). Differently, the initial state prepared in this case is more complicated. We switch on the dissipative channel (i.e., $|e\rangle \rightarrow |p\rangle \rightarrow |g\rangle$) and employ
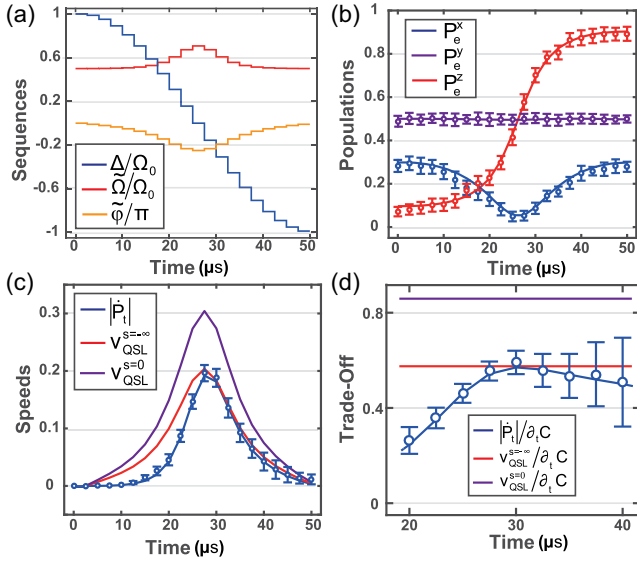
FIG. 3. Experimental implementation in the case of initially prepared TES, where the time period is fixed at 50 μs. The panels (a, b, c, d) here correspond, respectively, to (c, d, e, f) in the previous figure. The characteristic parameters are also the same as defined in the previous figure.

reinforcement learning to prepare the required TES [33]. The test of our proposed trade-off is executed similarly to the above case of initially pure state. From the observations in Figs. 3(c) and 3(d), we may draw the same conclusions as in the case of the initially pure state that $V_{QSL}^{s=-\infty}$ represents the optimal upper bound of the QSL and thus reaches the optimal trade-off.

In summary, we have established an optimal trade-off between the dynamical speed and the cost rate of the transitionless driving field in the context of shortcuts to adiabaticity, utilizing the *s*-parametrized phase space technique. We have justified both theoretically and experimentally that this novel trade-off stands out from previous relations by being tight. These findings substantially enhance our comprehension of the fundamental constraints inherent in quantum operations, underscoring the impossibility of arbitrarily fast processes. Moreover, the method and results of our work promote the understanding that less commonly utilized phase spaces, which have been largely overlooked, may offer superior advantages in certain quantum tasks.

*These authors contributed equally to this work.
†zhoufei@wipm.ac.cn
‡zhenyuxu@suda.edu.cn
§mangfeng@wipm.ac.cn

[1] D. Gúery-Odelin, A. Ruschhaupt, A. Kiely, E. Torrontegui, S. Martínez-Garaot, and J. G. Muga, Shortcuts to adiabaticity: Concepts, methods, and applications, Rev. Mod. Phys. **91,** 045001 (2019).

[2] M. Demirplak and S. A. Rice, Adiabatic population transfer with control fields, J. Phys. Chem. A **107,** 9937 (2003).

[3] M. Demirplak and S. A. Rice, Assisted adiabatic passage revisited, J. Phys. Chem. B **109,** 6838 (2005).

[4] M. V. Berry, Transitionless quantum driving, J. Phys. A **42,** 365303 (2009).

[5] X. Chen, A. Ruschhaupt, S. Schmidt, A. del Campo, D. Gúery-Odelin, and J. G. Muga, Fast optimal frictionless atom cooling in harmonic traps: Shortcut to adiabaticity, Phys. Rev. Lett. **104,** 063002 (2010).

[6] M. G. Bason, M. Viteau, N. Malossi, P. Huillery, E. Arimondo, D. Ciampini, R. Fazio, V. Giovannetti, R, Mannella, and O, Morsch1, High-fidelity quantum driving, Nat. Phys. **8,** 147 (2012).

[7] A. Ruschhaupt, X. Chen, D. Alonso, and J. G. Muga, Optimally robust shortcuts to population inversion in two-level quantum systems, New J. Phys. **14,** 093040 (2012).

[8] A. del Campo, Shortcuts to adiabaticity by counterdiabatic driving, Phys. Rev. Lett. **111,** 100502 (2013).

[9] J. F. Zhang, J. H. Shim, I. Niemeyer, T. Taniguchi, T. Teraji, H. Abe, S. Onoda, T. Yamamoto, T. Ohshima, J. Isoya, and Dieter Suter, Experimental implementation of assisted quantum adiabatic passage in a single spin, Phys. Rev. Lett. **110,** 240501 (2013).

[10] S. Campbell, G. De Chiara, M. Paternostro, G. M. Palma, and R. Fazio, Shortcut to Adiabaticity in the Lipkin-Meshkov-Glick model, Phys. Rev. Lett. **114,** 177206 (2015).

[11] S. An, D. Lv, A. del Campo, and K. Kim, Shortcuts to adiabaticity by counterdiabatic driving for trapped-ion displacement in phase space, Nat. Commun. **7,** 12999 (2016).

[12] Y. X. Du, Z. T. Liang, Y. C. Li, X. X. Yue, Q. X. Lv, W. Huang, X. Chen, H. Yan, and S. L. Zhu, Experimental realization of stimulated Raman shortcut-to-adiabatic passage with cold atoms, Nat. Commun. **7,** 12479 (2016).

[13] K. Takahashi, Shortcuts to adiabaticity for quantum annealing, Phys. Rev. A **95,** 012309 (2017).

[14] J. Cohn, A. Safavi-Naini, R. J. Lewis-Swan, J. G. Bohnet, M. Gärttner, K. A. Gilmore, J. E. Jordan, A. M. Rey, J. J. Bollinger, and J. K. Freericks, Bang-bang shortcut to adiabaticity in the Dicke model as realized in a Penning trap experiment, New J. Phys. **20,** 055013 (2018).

[15] J. KÖlbl, A. Barfuss, M. S. Kasperczyk, L. Thiel, A. A. Clerk, H. Ribeiro, and P. Maletinsky, Initialization of single spin dressed states using shortcuts to adiabaticity, Phys. Rev. Lett. **122,** 090502 (2019).

[16] H. Zhou, Y. L. Ji, X. F. Nie, X. D Yang, X, Chen, J. Bian, and X. H. Peng, Experimental realization of shortcuts to adiabaticity in a nonintegrable spin chain by local counterdiabatic driving, Phys. Rev. Applied **13**, 044059 (2020).

[17] Y. H. Chen, W. Qin, X, Wang, A, Miranowicz, and F. Nori, Shortcuts to adiabaticity for the quantum Rabi model: Efficient generation of giant entangled cat states via parametric amplification, Phys. Rev. Lett. **126**, 023602 (2021).

[18] S. Campbell and S. Deffner, Trade-off between speed and cost in shortcuts to adiabaticity, Phys. Rev. Lett. **118**, 100601 (2017).

[19] K. Funo, J. N. Zhang, C. Chatou, K. Kim, M. Ueda, and A. del Campo, Universal work fluctuations during shortcuts to adiabaticity by counterdiabatic driving, Phys. Rev. Lett. **118**, 100602 (2017).

[20] E. Torrontegui, I. Lizuain, S. González-Resines, A. Tobalina, A. Ruschhaupt, R. Kosloff, and J. G. Muga, Energy consumption for shortcuts to adiabaticity, Phys. Rev. A **96**, 022133 (2017).

[21] Z. X. Zhang, T. H. Wang, L. Xiang, Z. L Jia, P. Duan, W. Z. Cai, Z. Zhan, Z. W. Zong, J. L. Wu, L. Y. Sun, Y. Yin, and G. P. Guo, Experimental demonstration of work fluctuations along a shortcut to adiabaticity with a superconducting Xmon qubit, New J. Phys. **20**, 085001 (2018).

[22] O. Abah, M. Paternostro, and E. Lutz, Shortcut-to-adiabaticity quantum Otto refrigerator, Phys. Rev. Res. **2**, 023120 (2020).

[23] S. Alipour, A. Chenu, A. T. Rezakhani, and A. del Campo, Shortcuts to adiabaticity in driven open quantum systems: Balanced gain and loss and non-Markovian evolution, Quantum **4**, 336 (2020).

[24] G. Li, J. F. Chen, C. P. Sun, and H. Dong, Geodesic path for the minimal energy cost in shortcuts to isothermality, Phys. Rev. Lett. **128**, 230603 (2022).

[25] A. Soriani, E. Miranda, S. Deffner, and M. V. S. Bonanca, Shortcuts to thermodynamic quasistaticity, Phys. Rev. Lett. **129**, 170602 (2022).

[26] C. O. Marina, G. M. Juan, and M. G. Sofía, Shortcut-to-adiabaticity-like techniques for parameter estimation in quantum metrology, Entropy **22**, 1251 (2020).

[27] S. Iram, E. Dolson, J. Chiel, J. Pelesko, N. Krishnan, ö. Güngör, B. Kuznets-Speck, S. Deffner, E. Ilker, J. G. Scott, and M. Hinczewski, Controlling the speed and trajectory of evolution with counterdiabatic driving, Nat. Phys. **17**, 135 (2021).

[28] A. D. Cimmarusti, Z. Yan, B. D. Patterson, L. P. Corcos, L. A. Orozco, and S. Deffner, Environment-assisted speed-up of the field evolution in cavity quantum electrodynamics, Phys. Rev. Lett. **114**, 233602 (2015).

[29] G. Ness, M. R. Lam, W. Alt, D. Meschede, Y. Sagi, and A. Alberti, Observing crossover between quantum speed limits, Sci. Adv. **7**, eabj9119 (2021).

[30] M. R. Lam, N. Peter, T. Groh, W. Alt, C. Robens, D. Meschede, A. Negretti, S. Montangero, T. Calarco, and A. Alberti, Demonstration of quantum brachistochrones between distant states of an atom, Phys. Rev. X **11**, 011035 (2021).

[31] J. Howard, A. Lidiak, C. Jameson, B. Basyildiz, K. Clark, T. Zhao, M. Bal, J. Long, D. P. Pappas, M. Singh, and Z. Gong, Implementing two-qubit gates at the quantum speed limit, Phys. Rev. Res. **5**, 043194 (2023).

[32] W. Meng and Z. Xu, Quantum speed limits in arbitrary phase spaces, Phys. Rev. A **107**, 022212 (2023).

[33] See Supplemental Material at http://link.aps.org/supplemental/10.1103/PhysRevLett.132.213602 for more details on technical derivations of the tight quantum speed limit optimized over s-parametrized phase spaces, and experimental preparation of the thermal equilibrium state via reinforcement learning.

[34] J. Dziarmaga, Dynamics of a quantum phase transition: Exact solution of the quantum Ising model, Phys. Rev. Lett. **95**, 245701 (2005).

[35] A. del Campo, M. M. Rams, and W. H. Zurek, Assisted finite-rate adiabatic passage across a quantum critical point: Exact solution for the quantum Ising model, Phys. Rev. Lett. **109**, 115703 (2012).

[36] J. Johansson, M. H. S. Amin, A. J. Berkley, P. Bunyk, V. Choi, R. Harris, M. W. Johnson, T. M. Lanting, Seth Lloyd, and G. Rose, Landau-Zener transitions in a superconducting flux qubit, Phys. Rev. B **80**, 012507 (2009).

[37] A. Das, Non-classical role of potential energy in adiabatic quantum annealing, J. Phys. Conf. Ser. **143**, 012001 (2009).

[38] Y. J. Zheng, S. Campbell, G. De Chiara, and D. Poletti, Cost of counterdiabatic driving and work output, Phys. Rev. A **94**, 042132 (2016).

[39] R. Horn and C. Johnson, *Matrix Analysis* (Cambridge University Press, Cambridge, England, 1985).

[40] While a large number of metrics exist, the Bures fidelity often emerges as one of the preferred choices. Nevertheless, the QSL bound, defined in terms of the Bures angle $\mathcal{L}_t = \arccos |\langle \psi_0 | \psi_t \rangle|$ as outlined in Ref. [18], may not only exhibit a lack of tightness but also potentially contradict the true dynamics, as detailed in [33]. Furthermore, the computation of Bures angle for mixed states is usually very challenging. In this Letter, we will employ the relative purity [41–44] instead.

[41] K. M. R. Audenaert, Comparisons between quantum state distinguishability measures, Quantum Inf. Comput. **14**, 31 (2014).

[42] A. del Campo, I. L. Egusquiza, M. B. Plenio, and S. F. Huelga, Quantum speed limits in open system dynamics, Phys. Rev. Lett. **110**, 050403 (2013).

[43] D. A. Lidar, I. L. Chuang, and K. B. Whaley, Decoherence-free subspaces for quantum computation, Phys. Rev. Lett. **81**, 2594 (1998).

[44] B. Shanahan, A. Chenu, N. Margolus, and A. del Campo, Quantum speed limits across the quantum-to-classical transition, Phys. Rev. Lett. **120**, 070401 (2018).

[45] K. E. Cahill and R. J. Glauber, Ordered expansions in boson amplitude operators, Phys. Rev. **177**, 1857 (1969).

[46] K. E. Cahill and R. J. Glauber, Density operators and quasiprobability distributions, Phys. Rev. **177**, 1882 (1969).

[47] J. E. Runeson and J. O. Richardson, Generalized spin mapping for quantum-classical dynamics, J. Chem. Phys. **152**, 084110 (2020).

[48] R. P. Rundle and M. J. Everitt, Overview of the phase space formulation of quantum mechanics with application to quantum technologies, Adv. Quantum Technol. **4**, 2100016 (2021).

[49] L. Mandelstam and I. Tamm, J. Phys. USSR **9**, 249 (1945).

[50] For the case of initially mixed states, it is theoretically cumbersome to establish a concise functional relationship between the speed limit and the cost rate, i.e., $V_{\mathrm{QSL}}^{-\infty}[\partial_t C]$. Consequently, the ratio $V_{\mathrm{QSL}}^{-\infty}(t)/\partial_t C$ continues to be utilized, as it can be directly assessed through numerical simulations based on Eqs. (1) and (4).

[51] For the deviation of the actual dynamic speed from the curve of $V_{\mathrm{QSL}}^{s=-\infty}$, we emphasize that the tight QSL bound and the actual dynamical speed might not coincide at the midpoint of the driving interval. The coincidence time point between
the two curves completely relies on the driving Hamiltonian [e.g., the $g(t)$ function in the LZ model] and the actual manipulation (e.g., the operational sequences) involved in our experiment. In our case here, the QSL bounds for the LZ model, i.e., the purple and red curves, look nearly symmetrical, whereas the actual dynamical speed exhibits evident asymmetry before and after $t = 29$ μs. This asymmetry primarily accounts for the noticeable discrepancy between the QSL bound and the actual dynamical speed observed over the short time period. This clarification applies to Fig. 3(c).